A Multifractal Representation of the Small-Scale Structure in a Turbulent Plume

R. I. SYKES, R. S. GABRUK, AND D. S. HENN

ARAP Group, Titan Research and Technology Division, Titan Corporation, Princeton, New Jersey

(Manuscript received 29 August 1994, in final form 5 April 1995)

ABSTRACT

An improved method for representing the small-scale structure of a turbulent scalar field using fractal recursion techniques is described. The model generalizes the fractal successive refinement method described by Sykes and Gabruk to include a more realistic description of the pseudodissipation field, that is, the square of the scalar gradient. Turbulent dissipation fields are known to be multifractal, so a multifractal generation technique has been incorporated into the fractal refinement model to yield a scalar field with fractal isosurfaces but with a multifractal pseudodissipation field.

The model fields are compared with realizations from large-eddy simulations of turbulent scalar dispersion and shown to provide improved agreement with the small-scale structure. The simple combination of fractal and multifractal properties employed in the model also provides insight into the structure of the random scalar field. Finally, the generation technique is completely localized in physical space and is therefore applicable to inhomogeneous fields.

1. Introduction

The complex structure of the scalar concentration field as it is dispersed in a turbulent flow has been extensively studied using the techniques of fractal geometry. Initial attempts to characterize the concentration field were based on analyzing the "cloud boundary" from photographic data (e.g., Lovejoy 1982; Rys and Waldvogel 1986; Prasad and Sreenivasan 1990a) and used the classical perimeter–area relations or box-counting methods of fractal geometry (Mandelbrot 1982). For a fractal boundary, there is a power-law increase in the length of the boundary as it is increasingly resolved in finer detail. This type of analysis can only be applied to sets of points, in this case the boundary of a cloud, and cannot give a complete description of the function $c(\mathbf{x})$, that is, the concentration value as a function of spatial location $\mathbf{x}$. More recently, the multifractal has been introduced (Benzi et al. 1984; Frisch and Parisi 1985; Halsey et al. 1986; Meneveau and Sreenivasan 1987a) to characterize the behavior of intermittent fields such as the turbulent kinetic energy dissipation. The definition of a multifractal involves the functional behavior of the field, and therefore gives a more complete description than conventional fractal analysis.

While the fractal boundary analysis can be criticized as incomplete since it attempts to characterize a field through examination of level sets or isosurfaces, this is still the predominant description of the concentration field. Sreenivasan (1991) reviews many of the fractal turbulence results and makes a clear distinction between isosurface analysis of the concentration field and multifractal analysis of the dissipation field. The reason for the distinction lies in the nature of the multifractal spectrum, which is a way of describing the distribution of singularities in a field.

We now present a brief discussion of the multifractal spectrum. See Sreenivasan (1991) and Feder (1988) and references therein for greater detail. If we consider a measure of the field χ, for example, the scalar dissipation, the total measure inside a subregion Ω_r of characteristic size r (a sphere of radius r, for example) is given by

$$X_r = \int_{\Omega_r} \chi(\mathbf{x}) d^d x, \tag{1}$$

where the superscript d denotes the space dimensionality. For example, the set of points that constitute a line have a space dimensionality of 1. Similarly, the set of points that make up a surface or a sphere have a space dimensionality of 2 or 3, respectively. The multifractal formalism asserts that

$$\frac{X_r}{X_L} \sim \left(\frac{r}{L}\right)^{\alpha}, \tag{2}$$

where X_L represents the dissipation within the total domain Ω_L. The exponent α depends on the position of the subregion since the multifractal scaling is strictly local and is associated with the strength of singularities. This can be seen by noting that $X_r \sim r^{\alpha}$ implies χ

Corresponding author address: Dr. R. Ian Sykes, ARAP Group, Titan Research and Technology Division, 50 Washington Rd., P.O. Box 2229, Princeton, NJ 08543-2229.

$\sim r^{\alpha-d}$, which diverges for $\alpha < d$, with smaller values of α associated with narrower spikes. Assuming that the entire measure is made up of an infinite number of iso-α sets, one attempts to relate the number of r-sized subregions (or "boxes") with α-strength singularities in a bandwidth $d\alpha$:

$$N(\alpha)d\alpha \sim \rho(\alpha)\left(\frac{r}{L}\right)^{-f(\alpha)} d\alpha, \tag{3}$$

where $\rho(\alpha)$ is some α-dependent prefactor. Here, $f(\alpha)$ is the singularity or multifractal spectrum; it is analogous to the fractal dimension for simple self-similar measures [where $N(r) \sim r^{-D}$], but is a function of the singularity strength. (Thus, the measure is made up of a multiplicity of fractal sets or multifractals.)

This definition is appropriate for singular fields, such as the energy dissipation, where the classical power spectrum diverges at high wavenumber and the localization of the dissipation in the smallest scales is properly described by the multifractal spectrum. While this is precisely the measure required for description of the dissipation field, it is not appropriate for a scalar concentration field, which is usually finite at all wavenumbers and exhibits a convergent power spectrum.

Another way of examining a multifractal measure, which turns out to be convenient for analysis, is through moment exponents or generalized dimensions. Multifractal measures obey a power-law relationship given by (e.g., Prasad and Sreenivasan 1990b)

$$\sum \left(\frac{X_r}{X_L}\right)^q \sim \left(\frac{r}{L}\right)^{(q-1)D_q}, \tag{4}$$

where D_q can be identified as the generalized dimension of Hentschel and Procaccia (1983) and the sum is taken over all boxes of size r in the domain. For $q > 0$, the sum on the left is increasingly dominated by larger peaks as q increases, whereas for $q < 0$, the sum is increasingly dominated by regions that tend toward zero as q decreases. Halsey et al. (1986) show that the (q, D_q) analysis can be related to the multifractal spectrum by the following Legendre transform relations:

$$\alpha(q) = \frac{d}{dq}[(q-1)D_q] + 1 - d \tag{5a}$$

$$f[\alpha(q)] = q[\alpha(q) - 1 + d] - (q-1)D_q. \tag{5b}$$

The functional description of the dissipation field as a multifractal is more complete than the isosurface fractal description and has lead several researchers to the view that a scalar field should be constructed from a properly defined dissipation field. Thus, Wilson et al. (1991) and Tessier et al. (1993) invoke "fractional integration" to derive a scalar concentration field from a dissipation field that has been generated using multifractal techniques. Unfortunately, the definition of the dissipation as the square of the concentration gradient necessarily involves loss of information, and the concentration field cannot be determined without arbitrary assumptions. In fact, the fractional integration is carried out in Fourier space and does not maintain the correct local relation between the dissipation field and the concentration gradient.

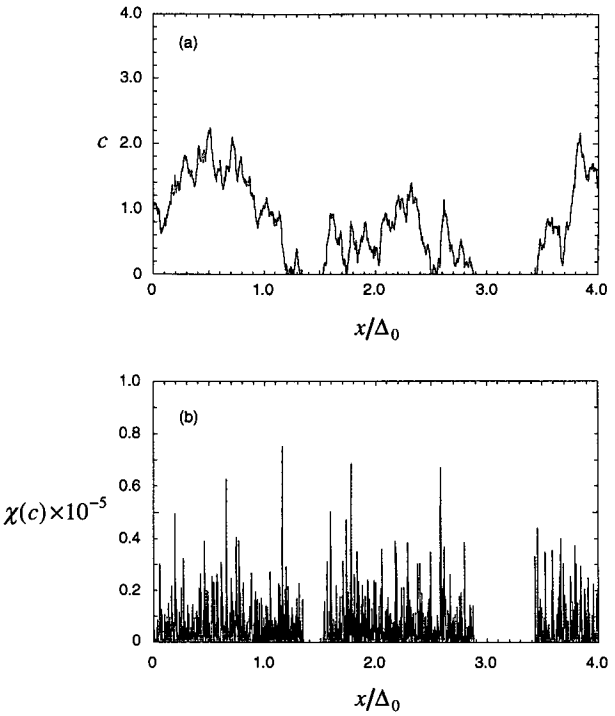

FIG. 1. One-dimensional recursive refinement fractal generation for a homogeneous concentration field with clipped-normal distribution and $\sigma_c/\bar{c} = 1$. Panel (a) shows the concentration field, panel (b) shows the dissipation field.

The correct relation between the concentration and dissipation fields can only be maintained by generating a scalar concentration field with the proper gradient behavior. We therefore begin with a technique for producing the concentration field and investigate ways of improving the dissipation field representation. The next section briefly reviews the fractal generation method of Sykes and Gabruk (1994) and examines the dissipation results from this simple model. Section 3 describes an extension of the model with an improved description of the dissipation field and compares the results with laboratory measurements of turbulent jets. In section 4, large-eddy simulations (LES) of a plume dispersing in a neutral boundary layer are analyzed and compared with the new model.

2. Recursive refinement model

Sykes and Gabruk (1994) present a fractal generation scheme for representing the scalar concentration field in a dispersing plume of material using the technique of successive refinement. The basic methodology consists of adding random pulses on successively

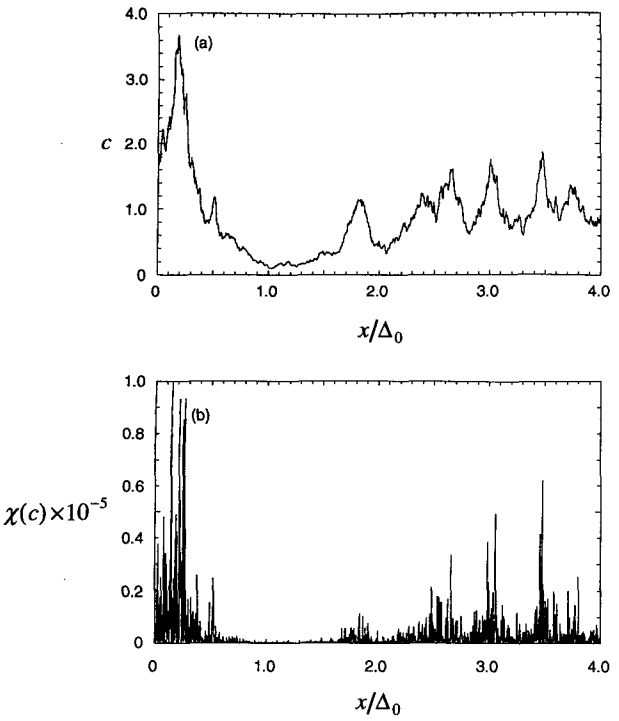

FIG. 2. Same as Fig. 1 except lognormal distribution.

smaller spatial scales with appropriately scaled variance, and is given in Voss (1988) and Feder (1988) as one of the methods for generating fractional Brownian motion. Sykes and Gabruk (1994) modify the original scheme to randomize the location of the pulses in order to give accurate representation of the scalar field variance. They show how the method can be adapted to represent an inhomogeneous field and can provide either lognormal or clipped-normal one-point probability density functions. The scheme is compared with LES results for turbulent plume dispersion from Sykes and Henn (1992) and Henn and Sykes (1992), and shown to give good agreement with the fractal isosurface results and also qualitative agreement with the instantaneous plume structure.

The fractal generation scheme for a homogeneous scalar field $c(\mathbf{x})$ can be written schematically in the form

$$c(x) = \bar{c} + \sum_n \sum_i a_{ni} P_n(x - x_{ni}), \qquad (6)$$

where the overbar denotes the ensemble average, n represents the refinement level, and i represents the range of overlapping pulse functions that contribute to the concentration fluctuation at the location x. The pulse function $P_n(x - x_{ni})$ is triangular in this scheme and centered at x_{ni} with a half-width of Δ_n, where $\Delta_n = 2^{-n}\Delta_0$. The pulse amplitude a_{ni} is chosen randomly from a Gaussian distribution with zero mean and standard deviation σ_n, where $\sigma_n = 2^{-nH}\sigma_0$. The relationship of the initial variance σ_0^2 to the ensemble variance is given in Sykes and Gabruk (1994). The fractal dimension of the field is controlled by the parameter H, which is the codimension, and is set to 0.65 based on the LES results. The fractal dimension of a level surface in a two-dimensional cross section is then $2 - H$; it is $1 - H$ for a time series. A nonnegative concentration field is generated by truncating negative values of c at zero (giving a clipped-normal distribution) or by exponentiating c (giving a lognormal distribution). The clipped-normal and lognormal parameters are defined in Sykes and Gabruk (1994).

Since it has been shown experimentally by Prasad et al. (1988) and Prasad and Sreenivasan (1990b) that the scalar dissipation field is multifractal, we now investigate the multifractal properties of the generated fields by examining the pseudodissipation field $\chi = (\delta c/\delta t)^2$. The recursive refinement model (6) can be implemented in arbitrary spatial dimension by defining the appropriate pulse functions P_n. Examples of one-dimensional concentration fields and the corresponding dissipation fields from clipped-normal and lognormal distributions with unit mean and variance

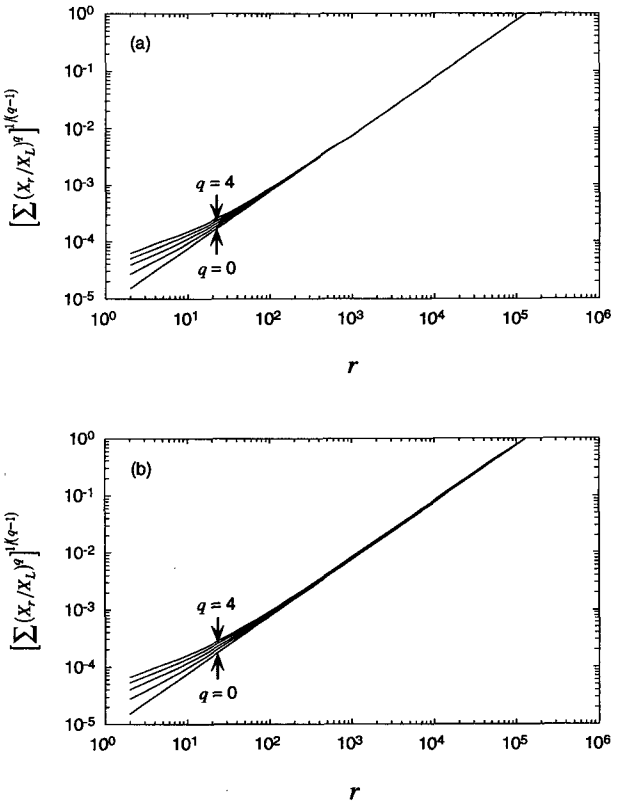

FIG. 3. Typical plot of $[\sum (X_r/X_L)^q]^{1/(q-1)}$ vs r for the dissipation field of a one-dimensional recursive refinement fractal generation for a homogeneous concentration field with $\sigma_c/\bar{c} = 1$. Panel (a) shows the clipped-normal distribution, panel (b) shows the lognormal distribution; $q = 0$, 1.02, 2, 3, and 4.

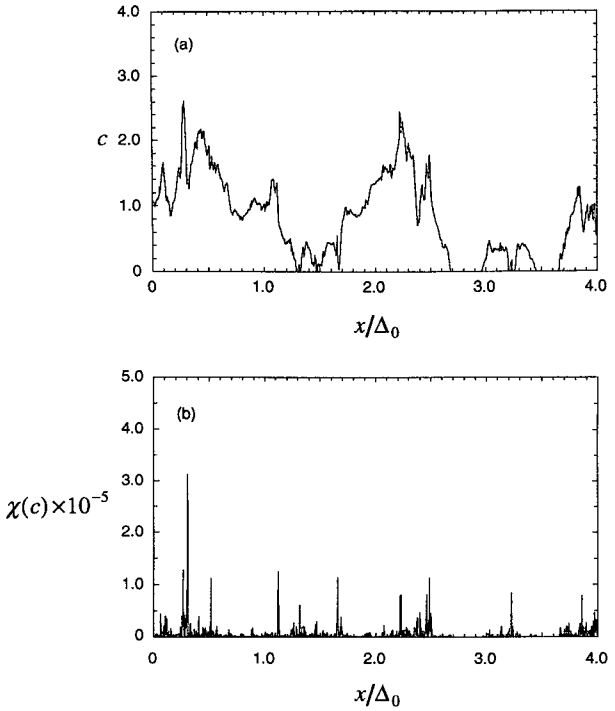

FIG. 4. One-dimensional recursive refinement multifractal generation for a homogeneous concentration field with clipped-normal distribution, $p = 0.8$, and $\sigma_c/\bar{c} = 1$. Panel (a) shows the concentration field, panel (b) shows the dissipation field.

are shown in Figs. 1 and 2, respectively. In these idealized cases, a periodic field is generated on a unit domain with an initial grid size of $\Delta_0 = 0.25$. The fields shown are typical fractal generation realizations. Other than the clipped regions, the scalar fields are quite similar. Furthermore, χ appears almost uniformly noisy except in areas of very low (or zero) concentration. This result is contrary to the intermittent character observed in various flow fields as noted in Prasad et al. (1988) and Prasad and Sreenivasan (1990b), and implies that the fractal model does not produce a multifractal dissipation field.

The absence of multifractal behavior is confirmed by a moment analysis of the dissipation field generated by the fractal model. Intermittent fields can be quantified by the behavior of various moments of the spatially averaged dissipation field as described in section 1. Using (4), we define

$$M_q(r) = \sum \left(\frac{X_r}{X_L}\right)^q, \qquad (7)$$

where X_r denotes the sum of χ over r time increments δt, and the sum is taken over all segments of size r in the domain. To demonstrate the use of (4) and (7) in multifractal analysis, one-dimensional realizations 1024 times longer than those shown in Figs. 1 and 2 were created. We could perform a multifractal analysis on the dissipation fields shown in the figures; however, a longer time series is more illuminating since it covers a wider scaling range. Figure 3 shows log–log plots of $M_q^{1/(q-1)}$ versus r for typical clipped-normal and lognormal realizations. The moment curves of a multifractal measure appear linear when plotted in this way so the slope of the log–log curve then gives the generalized dimension D_q. Only the positive moments are shown because M_q is undefined for $q < 0$ when $c = 0$ for the clipped-normal distribution. For the larger scales, the moment curves indicate nonfractal behavior since they show the same slope of D_q for all q. However, at the smaller scales, the curves diverge and appear to be nonlinear. (This may be due to numerical resolution problems rather than indicating any scaling behavior.) These results are in contrast to the experimental observations of Prasad et al. (1988) and Prasad and Sreenivasan (1990b). Therefore, a different generation scheme is required to produce a dissipation field that is consistent with those observations.

3. Generation of a multifractal dissipation field

Multifractal fields can be generated using a very simple multiplicative cascade process. This method has been applied in the so-called "p model" of the turbulent kinetic energy dissipation field structure by Meneveau and Sreenivasan (1987b). The p model simply involves unequal division of an initially uniform field among the subdivided cells in a recursive refinement process.

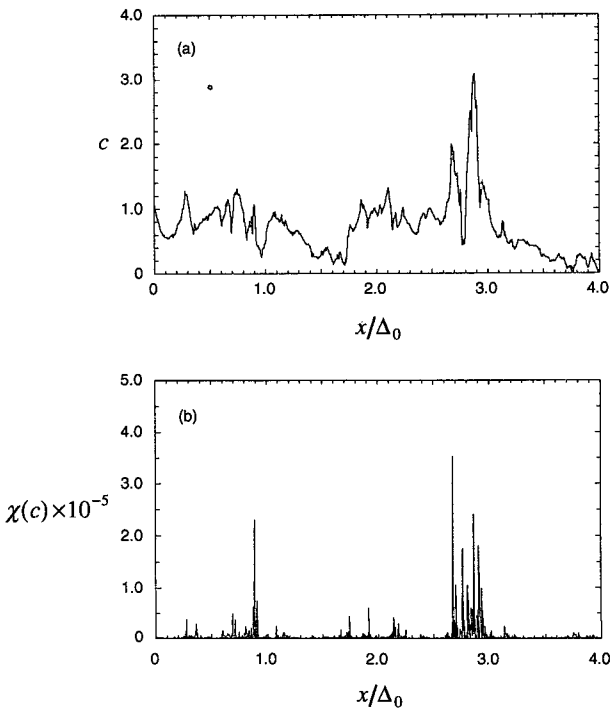

FIG. 5. Same as Fig. 4 except lognormal distribution.

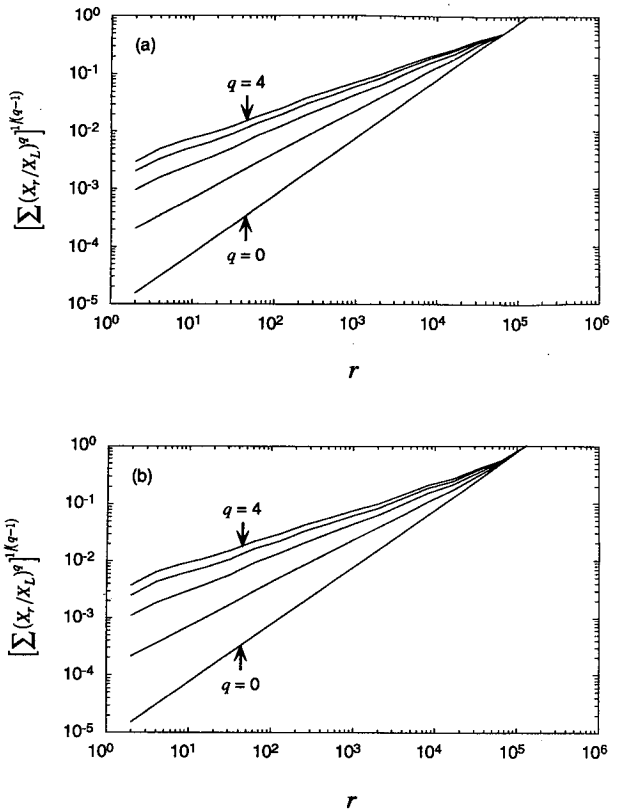

FIG. 6. Typical plot of $[\Sigma\ (X_r/X_L)^q]^{1/(q-1)}$ vs r for the dissipation field of a one-dimensional recursive refinement multifractal generation for a homogeneous concentration field with $p = 0.8$ and $\sigma_c/\bar{c} = 1$. Panel (a) shows the clipped-normal distribution, panel (b) shows the lognormal distribution; $q = 0$, 1.02, 2, 3, and 4.

Thus, in a one-dimensional model, when a cell is divided into two equal-length subcells, one cell receives a fraction p of the value in the original cell, while the other receives a fraction $1 - p$. The process is randomized by assigning the fraction p to either cell with probability 0.5; it is assumed that $0.5 \leq p \leq 1.0$. The process is repeated with fixed p until the smallest scale is reached. This model concentrates the dissipation field into localized regions and has been shown to give a multifractal (Benzi et al. 1984).

The p model is useful for generating a representation of the dissipation field, but our objective is the generation of a scalar concentration field that possesses the proper dissipation field structure. As mentioned in section 1, Wilson et al. (1991) and Tessier et al. (1993) have used the multifractal representation of the dissipation field to obtain a scalar concentration field by means of "fractional integration." The procedure is apparently an arbitrary filtering technique and it does not preserve the local definition of the dissipation as the square of the concentration gradient. Furthermore, it is also performed in Fourier space, which makes its application to inhomogeneous fields difficult. The p model, on the other hand, is completely localized in space and we therefore seek to incorporate some of the features of the p model into the recursive refinement technique [Eq. (6)] as a means of improving the dissipation field representation.

The basis of the refinement technique is the addition of random pulses at each of a succession of smaller scales with the amplitude of the pulses chosen randomly from a specified distribution. The fractal dimension of the field is determined by the rate at which the distribution variance decreases with the scale of the pulses. This procedure clearly allocates fluctuation variance uniformly among the pulses at each scale and produces the nonintermittent dissipation result illustrated in Figs. 1b and 2b. We can generate intermittency in the small scales responsible for the dissipation by using the p model to allocate variance at each level of refinement. Thus, instead of simply defining

$$\sigma_{n+1}^2 = 2^{-2H}\sigma_n^2, \tag{8}$$

where n refers to the refinement level, we define a local value for each pulse as

$$\sigma_{n+1}^2 = 2^{1-2H}\sigma_n^2 p', \tag{9}$$

where p' is randomly chosen from the pair $(p, 1 - p)$, and σ_n^2 refers to the variance in the "parent" cell of the refinement. Each parent cell is divided into 2^d "offspring" cells, with half allocated the variance defined by (9) and the other half allocated a similar variance but with p' replaced by $1 - p'$. The p' factor is multiplicative since it is applied at each level of refinement, but the ensemble average variance is conserved by (9). The variance definition contains a factor $2p'$, which clearly has an average value of unity. Allocating variance in this way is similar to the bounded cascade model of Marshak et al. (1994); however, the actual scalar field construction is quite different.

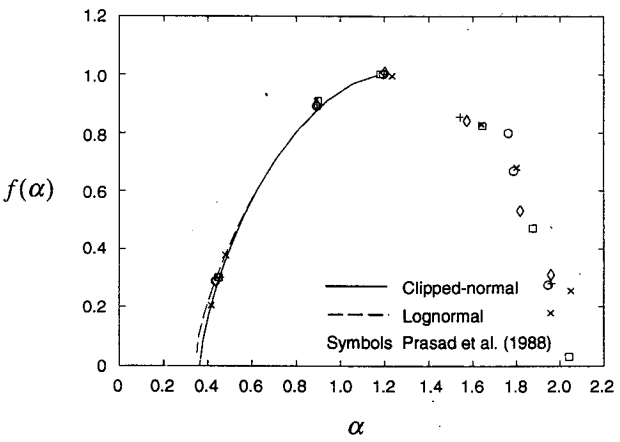

FIG. 7. Multifractal spectra from the averaged D_q curves of the dissipation fields of 100 one-dimensional recursive refinement multifractal realizations for a homogeneous concentration field with $p = 0.8$ and $\sigma_c/\bar{c} = 1$.

The scheme defined by (6) and (9) consists of a sum of pulses with random amplitudes drawn from a local distribution determined by a multiplicative process. That is, the p model is used to determine the local variance for the random pulse amplitude, and therefore the smaller scales can be expected to become increasingly intermittent. On the other hand, the concentration field is obtained from the sum of all the pulses and so will not be dominated by small-scale intermittency. The sum is convergent everywhere provided $p < 2^{2H-1}$, which is trivially satisfied if $H > 0.5$. Examples of time series ($d = 1$) generated by the new model with $p = 0.80$ are presented in Figs. 4 and 5. The value of 0.80 was chosen to give a good fit to the multifractal spectrum (shown below) measured by Prasad et al. (1988). It is close to the value of 0.70 used by Meneveau and Sreenivasan (1987b) in modeling the turbulent kinetic energy dissipation, and 0.75 mentioned by Sreenivasan (1991) for scalar dissipation, although in these cases the actual dissipation rates are being split instead of variance. The concentration time series look similar to the fractal model results in Figs. 1a and 2a, but the χ realizations are clearly more intermittent. The intermittency is confirmed by the moment analysis, shown in Fig. 6, which now shows evidence of multifractal structure. Typical log–log plots of the moment curves show distinct linear regions over four orders of magnitude as well as a variation of slope with q, in contrast the original fractal model results. As with the original fractal model analysis, time series 1024 times longer than those shown in the figures were used

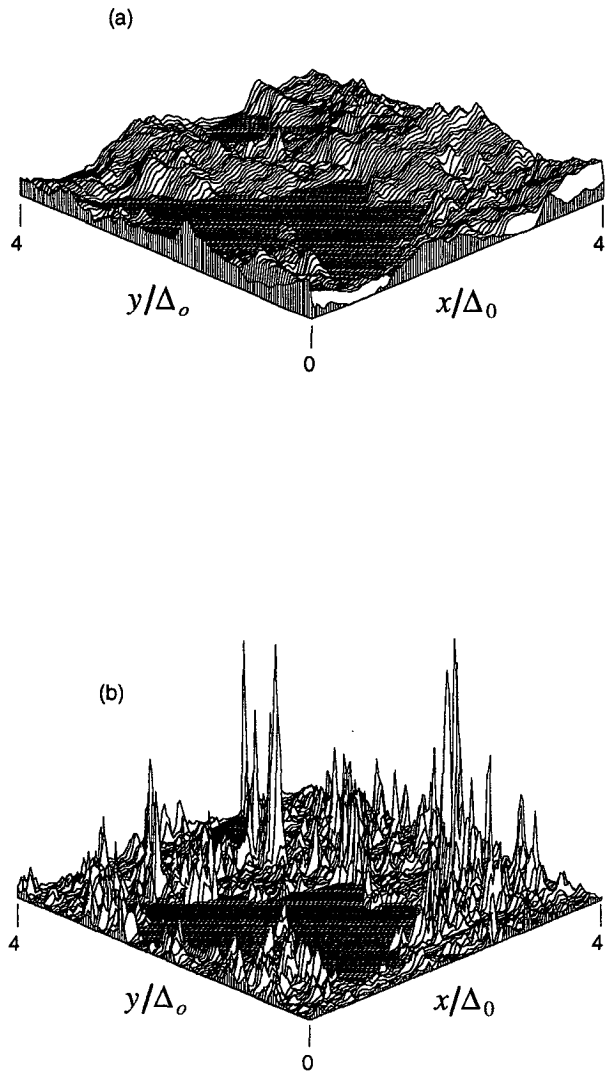

FIG. 8. Two-dimensional recursive refinement multifractal generation for a homogeneous concentration field with clipped-normal distribution, $p = 0.8$, and $\sigma_c/\bar{c} = 1$. The vertical axes are scaled arbitrarily. Panel (a) shows the concentration field, panel (b) shows the dissipation field.

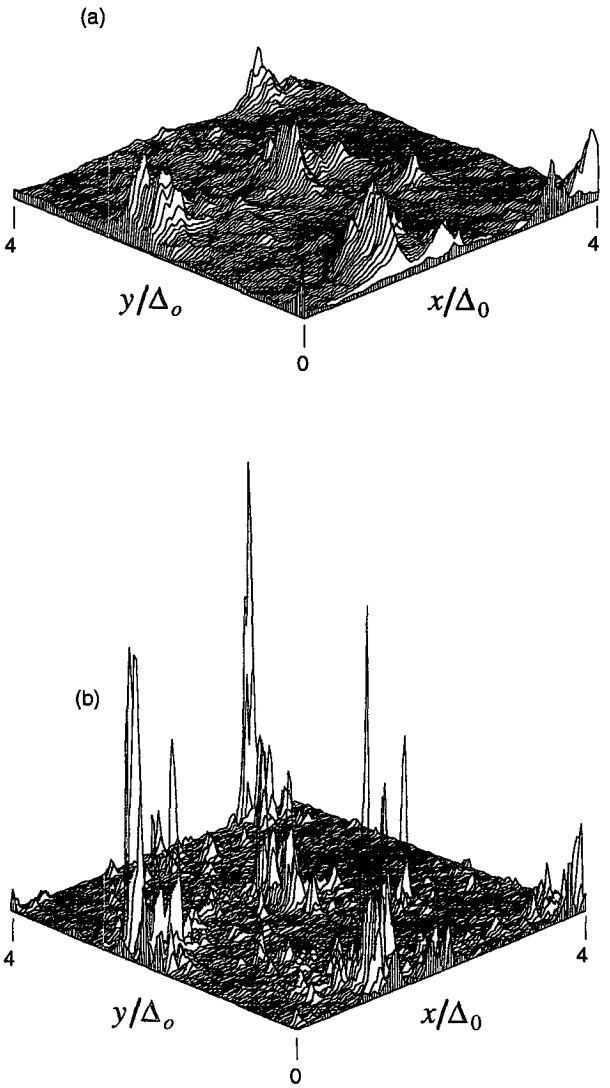

FIG. 9. Same as Fig. 8 except lognormal distribution.

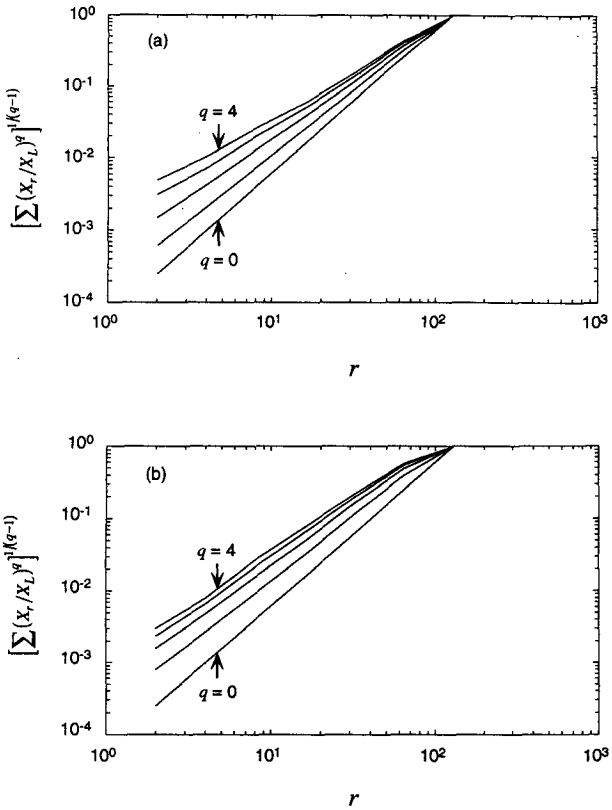

FIG. 10. Typical plot of $[\sum (X_r/X_L)^q]^{1/(q-1)}$ vs r for the dissipation field of a two-dimensional recursive refinement multifractal generation for a homogeneous concentration field with $p = 0.8$ and $\sigma_c/\bar{c} = 1$. Panel (a) shows the clipped-normal distribution, panel (b) shows the lognormal distribution; $q = 0$, 1.02, 2, 3, and 4.

to compute the moment curves. The linear range appears to hold down to $r \approx 4$, that is, 2 times the smallest pulse width. Below this size, the number of grid refinements is inadequate to make reliable estimates of M_q.

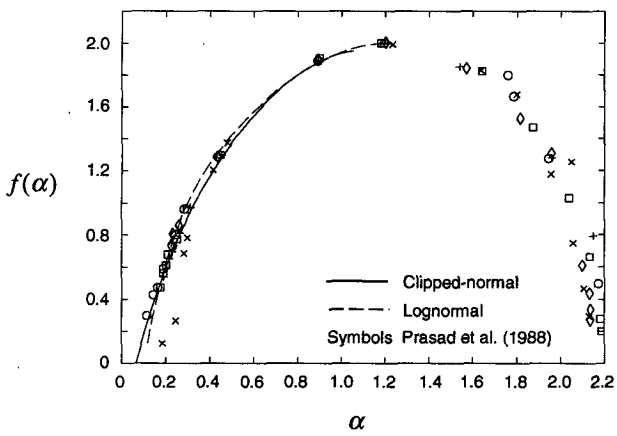

FIG. 11. Multifractal spectra from the averaged D_q curves of the dissipation fields of 25 two-dimensional recursive refinement multifractal realizations for a homogeneous concentration field with $p = 0.8$ and $\sigma_c/\bar{c} = 1$.

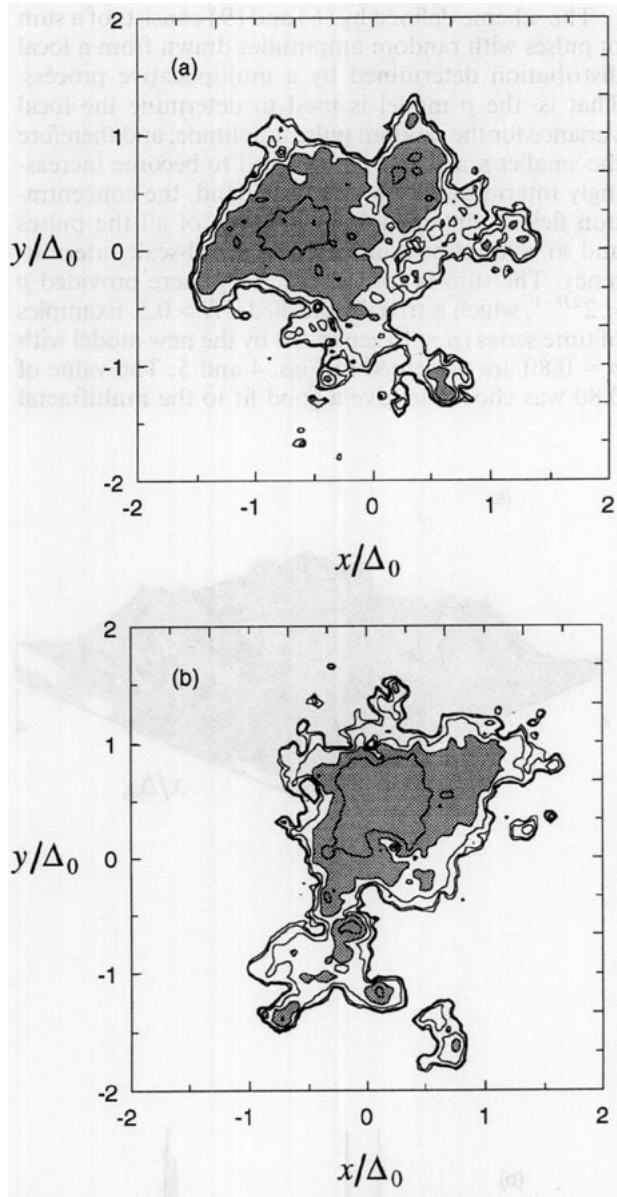

FIG. 12. Two-dimensional recursive refinement fractal and multifractal realizations for an inhomogeneous concentration field with clipped-normal distribution and $(\sigma_c/\bar{c})_{max} = 1$. Panel (a) shows the fractal model, panel (b) shows the multifractal model.

The model-generated multifractal spectra $f(a)$ for both the clipped-normal and lognormal distributions are shown in Fig. 7. These are determined using (5a) and (5b) with averaged estimates of D_q from 100 realizations. The multifractal generation scheme gives a very good representation of the spectrum of Prasad et al. (1988). This is important since Prasad and Sreenivasan (1990b) suggest that the scalar dissipation multifractal spectrum is universal for high Reynolds numbers based on turbulent jet and wake experiments.

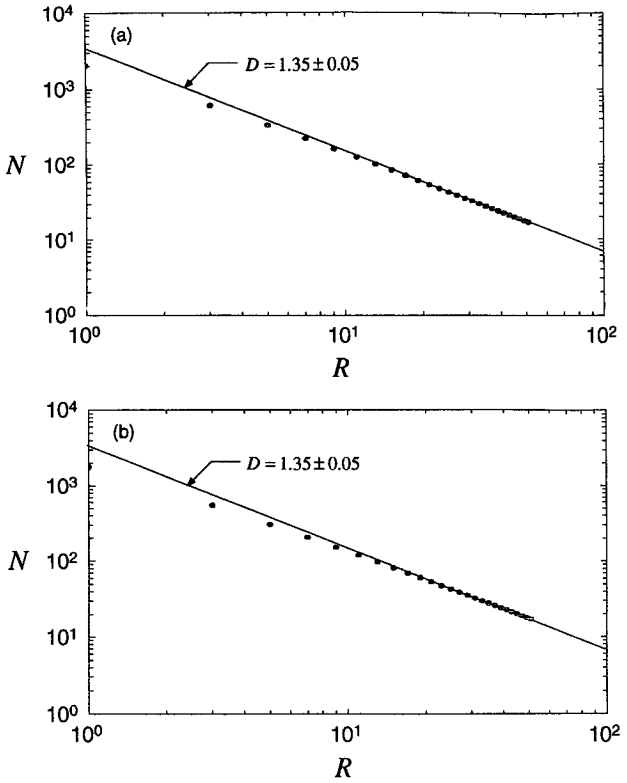

FIG. 13. Box-counting analyses of fractal and multifractal generation for an inhomogeneous concentration field with clipped-normal distribution and $(\sigma_c/\bar{c})_{\max} = 1$. Panel (a) shows the fractal model, panel (b) shows the multifractal model.

Similarly, Meneveau and Sreenivasan (1987a, 1991) show the universality of the kinetic energy dissipation multifractal spectrum based on measurements from wind tunnel boundary layers, wakes, grid turbulence, and the atmospheric surface layer.

The analysis of the complete multifractal model is complicated by the summation of the random pulses from a multiplicative cascade process. However, the multifractal behavior of the pseudodissipation field can be understood as a result of the emphasis of the small scales by the gradient operator. Although the series for the concentration field is convergent, provided $p < 2^{2H-1}$, the series for the concentration gradient is divergent for $H < 1$. The dissipation field is therefore dominated by the smallest scales under consideration and exhibits the properties of the standard p model without summation. The concentration field itself is nonsingular and is more strongly influenced by the larger-scale features that contain more variance.

As given above, (6) and (9) are applicable to higher dimensions, so we now examine two-dimensional plume cross sections generated by the multifractal model. Realizations of c and χ from the clipped-normal and lognormal distributions are shown in Figs. 8 and 9. The clipped-normal scalar field is characterized by broad areas of either fairly high or zero concentration. The lognormal distribution results in relatively few isolated regions of high concentration surrounded by broad areas of small (but nonzero) concentration. The pseudodissipation fields from both distributions show many narrow spikes, but the lognormal distribution tends to produce them in the isolated regions associated with higher concentration levels. The distribution of spikes in χ from the clipped-normal distribution tends to mirror that of c in that are they fairly uniformly distributed over the regions where $c > 0$.

The multifractal moment curves from the two-dimension simulations are given in Fig. 10 and the resulting multifractal spectra in Fig. 11. The moment curves are determined from realizations in a domain 4 times that shown in Figs. 8 and 9. The multifractal spectra are averages from 25 such realizations. The moment curves show well-defined linear regions over approximately two decades, allowing estimates of D_q. The multifractal spectra for the two distributions are quite similar and also show good agreement with the spectrum presented in Prasad et al. (1988). So although both clipped-normal and lognormal distributions produce fields consistent with the universal spectrum, the

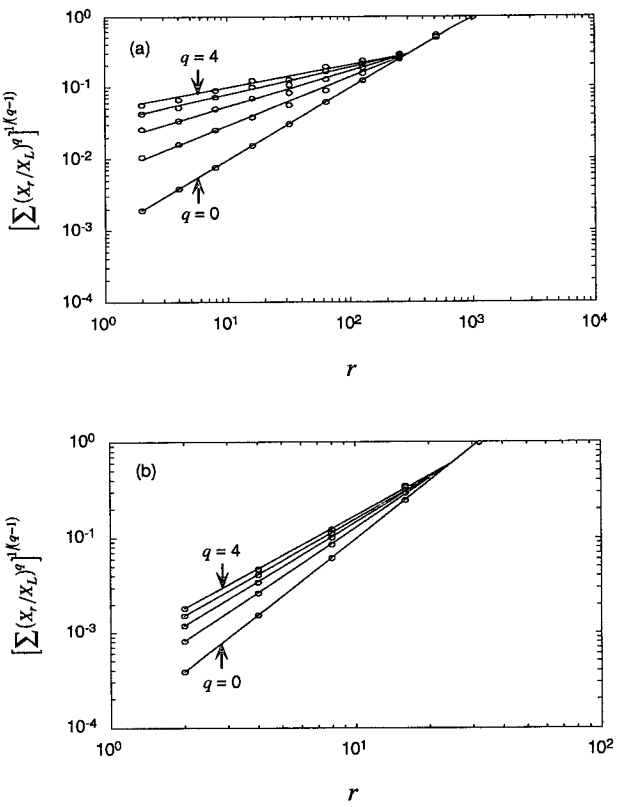

FIG. 14. Typical plots of $[\sum (X_r/X_L)^q]^{1/(q-1)}$ vs r for the dissipation field of one and two-dimensional LES neutral boundary realizations. Panel (a) shows the time series, panel (b) shows the plume cross section.

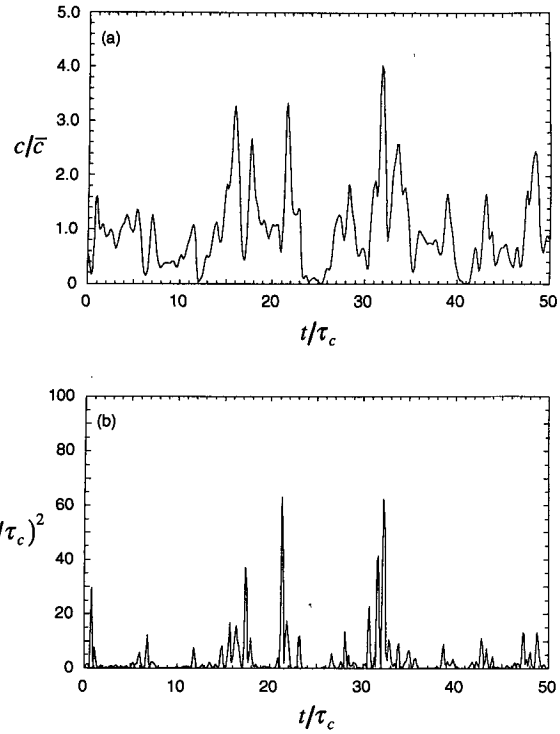

FIG. 15. LES neutral boundary layer time series at $x/\delta = 6.67$ on the plume centerline. The LES autocorrelation timescale and the LES mean concentration are represented by τ_c and $\bar{c}$, respectively. Panel (a) shows the concentration field, panel (b) shows the dissipation field.

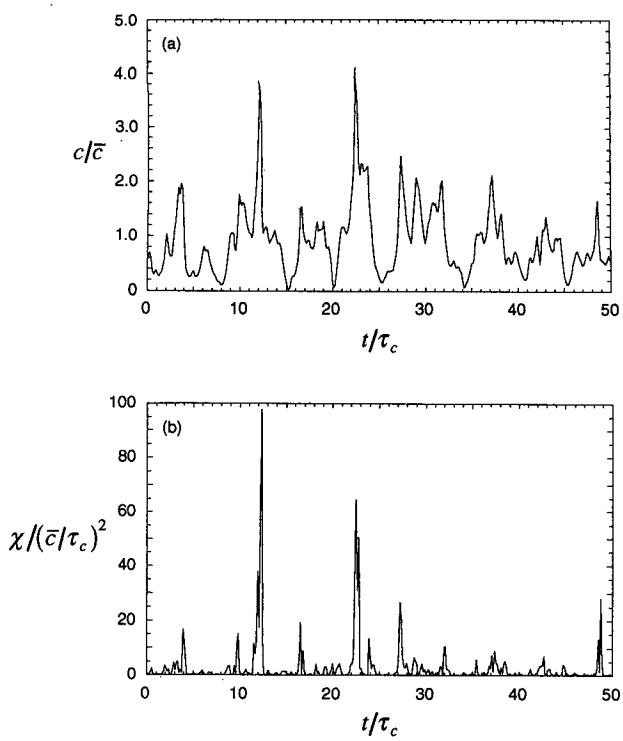

FIG. 16. One-dimensional recursive refinement multifractal simulation of the LES neutral boundary layer time series shown in Fig. 15. The terms τ_c and $\bar{c}$ are the same as in Fig. 15. Panel (a) shows the concentration field, panel (b) shows the dissipation field.

pseudodissipation fields do have somewhat different characteristics. Thus, it is important that the correct distribution be known.

So far we have only investigated the multifractal behavior of the dissipation field of our new multifractal generation scheme. However, we are also interested in preserving the fractal behavior of the original model (Sykes and Gabruk 1994). That is, a given isoconcentration contour has a fractal dimension that is consistent with the given codimension H. Typical realizations of idealized inhomogeneous fields (i.e., a Gaussian concentration distribution) for the fractal and multifractal models are shown in Fig. 12. In these realizations,

$$\bar{c} = e^{-(x^2+y^2)}$$

$$\overline{c'^2} = \sigma_c^2 e^{-(x^2+y^2)},$$

where the overbar denotes ensemble mean and the prime denotes fluctuation from the mean. We generate the representation for $x \in [-3,3]$ and $\Delta_0 = 1.5$. We also use a unit σ_c. The mass and fractal dimension of the realizations are virtually identical. The basic structure of the multifractal field is very similar to that of the original fractal model; however, there are subtle differences in the very small-scale behavior. The fractally generated field exhibits more small "islands" than that of the multifractal model even though the fractal dimension is the same. Thus, the two models have slightly different lacunarity (Mandelbrot 1982).

Box-counting results for the scalar fields of the fractal and multifractal models are shown in Fig. 13. The

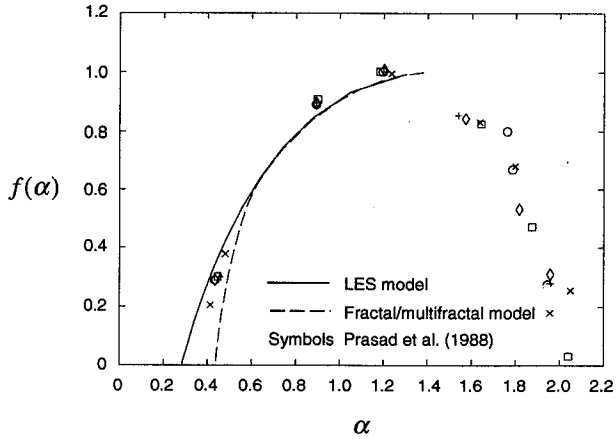

FIG. 17. Multifractal spectra from the averaged D_q curves of the dissipation fields of 5 LES one-dimensional realizations and 100 one-dimensional recursive refinement multifractal realizations with log-normal distribution.

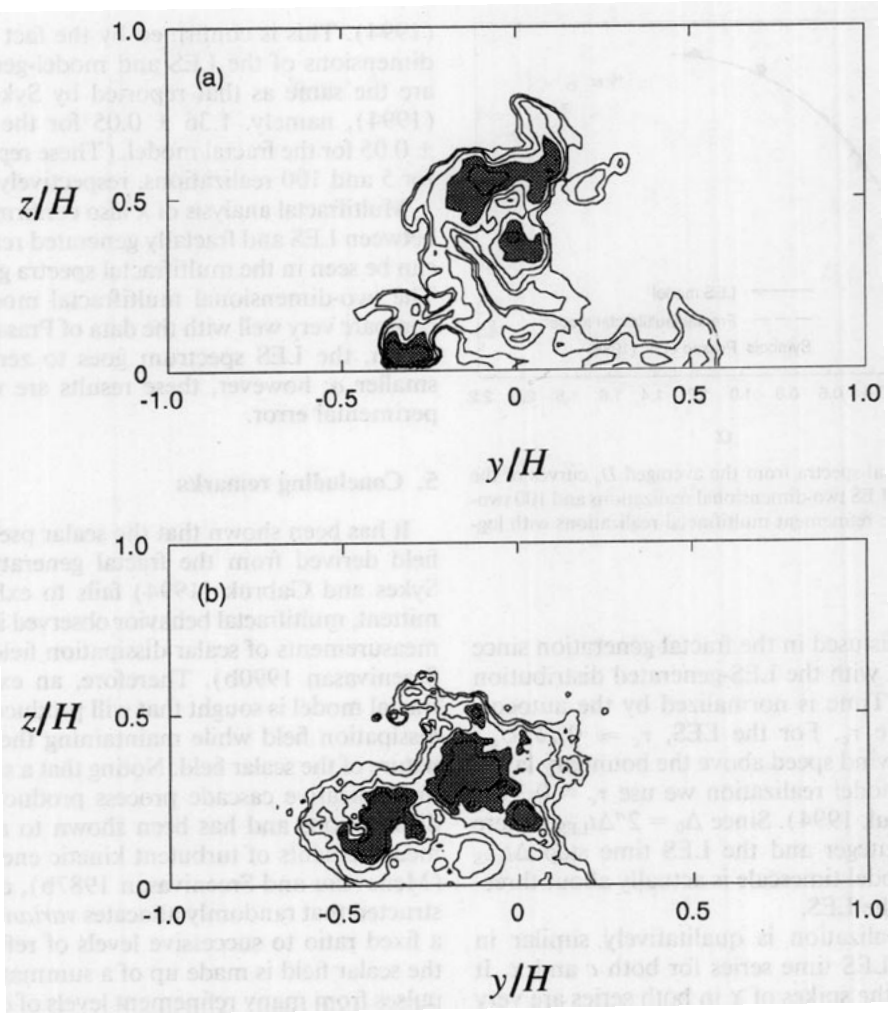

FIG. 18. Neutral boundary layer plume realizations of c normalized by the maximum mean concentration at $x/\delta = 5$. Contours are 0.1, 0.2, 0.5, 1, 2, and 5. Stippled areas are equal to or greater than 1. Panel (a) shows the LES model, panel (b) shows the multifractal model.

fractal analysis was performed on concentration isopleths for realizations with a resolution that is twice that shown in Fig. 12. An isopleth threshold value of 0.1 was chosen as a representative value for the edge of the plume. This value must be small enough to give an extensive contour but not so small that numerical errors are significant. See Sykes and Gabruk (1994) for more information on box counting. The box-counting results are averages from 100 such realizations for each model. Both plots demonstrate self-similarity over most of the scaling range with a fractal dimension of 1.35 ± 0.05.

4. Comparison with LES data

Sykes and Gabruk (1994) present a fractal analysis of the LES neutral boundary layer plume calculations of Sykes and Henn (1992). That analysis is augmented here by examining the LES-generated pseudodissipation field and comparing it with realizations generated with the new multifractal model. However, it should be noted that the LES results only cover a limited scaling range of just over two decades and one decade for one- and two-dimensional realizations, respectively. Therefore, estimates of the generalized dimensions are not as reliable as in the idealized cases presented in the previous section. The multifractal moment curves from typical one- and two-dimensional LES realizations are shown in Fig. 14.

Figures 15 and 16 show one-dimensional time series of c and χ from the LES calculations and a realization generated with the new technique, respectively. The LES time series is taken from a location on the plume centerline at $x/\delta = 6.67$ (x is the downstream distance from the source) and at the release height of 0.19δ, where δ is the boundary layer height. The fluctuation intensity ratio $\sigma_c/\bar{c}$ is 1, where σ_c is the standard deviation of the concentration fluctuations. The lognor-

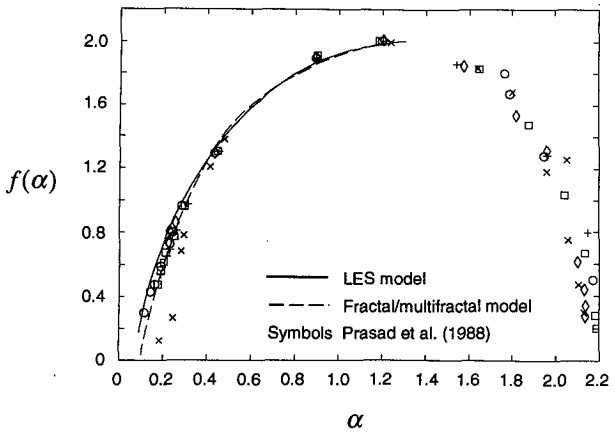

FIG. 19. Multifractal spectra from the averaged D_q curves of the dissipation fields of 5 LES two-dimensional realizations and 100 two-dimensional recursive refinement multifractal realizations with log-normal distribution.

mal distribution is used in the fractal generation since that is consistent with the LES-generated distribution at this location. Time is normalized by the autocorrelation timescale τ_c. For the LES, $\tau_c \approx 0.2\delta/U_\infty$, where U_∞ is the wind speed above the boundary layer. For the fractal model realization we use $\tau_c = 0.33\Delta_0$ (Sykes and Gabruk 1994). Since $\Delta_0 = 2^n\Delta t_{\text{LES}}$, where n is a positive integer and the LES time step $\Delta t_{\text{LES}} \approx 0.14\tau_c$, the model timescale is actually about three-quarters that of the LES.

The fractal realization is qualitatively similar in character to the LES time series for both c and χ. It can be seen that the spikes of χ in both series are very similar in frequency, duration, and amplitude. The similarities are confirmed by the multifractal spectra given in Fig. 17. These multifractal results also compare very well with the data of Prasad et al. (1988). The LES spectrum goes to zero at slightly smaller α than the model or experimental spectra, indicating a more intermittent dissipation field. However, given the limited scaling range and the concomitant uncertainty in D_q, the LES spectrum is reasonably close to the experimental results.

Analyzing two-dimensional LES plume cross sections and the corresponding multifractal model realizations is somewhat problematic since the cross sections are inhomogeneous and the multifractal analysis is strictly valid only for homogeneous fields. Therefore, relatively small boxes (32 × 32 LES grid cells) fully contained within the plume are used for analysis so that the regions are "nearly" homogeneous. An LES-generated plume cross section at $x/\delta = 5$ and a corresponding model realization are shown in Fig. 18. It should be noted that the model realization uses the local mean and variance determined from LES. The realizations appear similar to one another as well as to the simple fractal model results in Sykes and Gabruk (1994). This is confirmed by the fact that the fractal dimensions of the LES and model-generated plumes are the same as that reported by Sykes and Gabruk (1994), namely, 1.36 ± 0.05 for the LES and 1.30 ± 0.05 for the fractal model. (These represent averages for 5 and 100 realizations, respectively.)

Multifractal analysis of χ also confirms the similarity between LES and fractally generated realizations. This can be seen in the multifractal spectra given in Fig. 19. The two-dimensional multifractal model results also compare very well with the data of Prasad et al. (1988). Again, the LES spectrum goes to zero at a slightly smaller α; however, these results are well within experimental error.

5. Concluding remarks

It has been shown that the scalar pseudodissipation field derived from the fractal generation scheme of Sykes and Gabruk (1994) fails to exhibit the intermittent, multifractal behavior observed in experimental measurements of scalar dissipation fields (Prasad and Sreenivasan 1990b). Therefore, an extension to the fractal model is sought that will produce a multifractal dissipation field while maintaining the simple fractal nature of the scalar field. Noting that a simple binomial multiplicative cascade process produces intermittent distributions and has been shown to agree well with measurements of turbulent kinetic energy dissipation (Meneveau and Sreenivasan 1987b), a model is constructed that randomly allocates *variance* unequally in a fixed ratio to successive levels of refinement. Since the scalar field is made up of a summation of random pulses from many refinement levels of decreasing variance, it is dominated by the larger-scale structures that contain most of the variance. The fractal behavior of the scalar field is maintained since the average variance at each level of iteration is still controlled by the codimension and, thus, the power spectra remains unchanged. However, the gradient operator involved in calculating the pseudodissipation field emphasizes small scales. In fact, the summation of pulse *gradients* diverges, so that the pseudodissipation field becomes highly intermittent and exhibits multifractal behavior. An important feature of the model is that it is completely local so that it may be applied to inhomogeneous fields.

Idealized time series are generated with the new multifractal model using clipped-normal and lognormal distributions to define the pulses. An analysis of these shows that the resulting multifractal spectra agree very well with the (assumed) universal spectrum derived from measurements of turbulent jets and wakes (Prasad and Sreenivasan 1990b), even though the pseudodissipation fields from the two distributions are somewhat different in character.

An analysis of LES neutral boundary layer plumes shows that the pseudodissipation fields reveal multi-

fractal behavior, although the scaling range is limited. Application of the multifractal model using the LES statistics yields plumes realizations that are similar in appearance to the LES realizations. The fractal dimensions of plume isosurfaces from the LES and model are close (1.36 and 1.30, respectively); the model dimension is unchanged from the simple fractal model results given in Sykes and Gabruk (1994). The LES multifractal spectrum is close to the model and experimental spectra, although it may indicate less intermittency in the LES pseudodissipation fields. However, given the uncertainty resulting from the small scaling range, the match with the presumed universal spectrum is reasonably good.

Acknowledgments. This work was supported by the Army Research Office under Contract DAAL03-92-C-0020.

REFERENCES

Benzi, R., G. Paladin, G. Parisi, and A. Vulpiani, 1984: On the multifractal nature of fully developed turbulence and chaotic systems. *J. Phys. A,* **17,** 3521–3531.

Feder, J., 1988: *Fractals.* Plenum, 283 pp.

Frisch, U., and G. Parisi, 1985: On the singularity of fully developed turbulence. *Turbulence and Predictability in Geophysical Fluid Dynamics and Climate Dynamics,* M. Ghil, R. Benzi, and G. Parisi, Eds., North-Holland.

Halsey, T. C., M. H. Jensen, L. P. Kadanoff, I. Procaccia, and B. I. Shraiman, 1986: Fractal measures and their singularities: The characterization of strange sets. *Phys. Rev. A,* **33,** 1141–1151.

Henn, D. S., and R. I. Sykes, 1992: Large-eddy simulation of dispersion in the convective boundary layer. *Atmos. Environ.,* **26A,** 3145–3159.

Hentschel, H. G. E., and I. Procaccia, 1983: Fractal nature of turbulence as manifested in turbulent diffusion. *Phys. Rev. A,* **27,** 1266–1269.

Lovejoy, S., 1982: Area–perimeter relation for rain and cloud areas. *Science,* **216,** 185–187.

Mandelbrot, B. B., 1982: *The Fractal Geometry of Nature.* W. H. Freeman and Co., 468 pp.

Marshak, A., A. Davis, R. Cahalan, and W. Wiscombe, 1994: Bounded cascade models as nonstationary multifractals. *Phys. Rev. E,* **49,** 55–69.

Meneveau, C., and K. R. Sreenivasan, 1987a: The multifractal spectrum of the dissipation field in turbulent flows. *Nucl. Phys. B (Proc. Suppl.),* **2,** 49–76.

——, and ——, 1987b: Simple multifractal cascade model for fully developed turbulence. *Phys. Rev. Lett.,* **59,** 1424–1427.

——, and ——, 1991: The multifractal nature of turbulent energy dissipation. *J. Fluid Mech.,* **224,** 429–484.

Prasad, R. R., and K. R. Sreenivasan, 1990a: The measurement and interpretation of fractal dimensions of surfaces in turbulent flows. *Phys. Fluids A,* **2,** 792–807.

——, and ——, 1990b: Quantitative three-dimensional imaging and the structure of passive scalar fields in fully turbulent flows. *J. Fluid Mech.,* **216,** 1–34.

——, C. Meneveau, and K. R. Sreenivasan, 1988: Multifractal nature of the dissipation field of passive scalars in fully turbulent flows. *Phys. Rev. Lett.,* **61,** 74–77.

Rys, F. S., and A. Waldvogel, 1986: Fractal shape of hail clouds. *Phys. Rev. Lett.,* **56,** 784–787.

Sreenivasan, K. R., 1991: Fractals and multifractals in fluid turbulence. *Annu. Rev. Fluid Mech.,* **23,** 539–600.

Sykes, R. I., and D. S. Henn, 1992: Large-eddy simulation of concentration fluctuations in a dispersing plume. *Atmos. Environ.,* **26A,** 3127–3144.

——, and R. S. Gabruk, 1994: Fractal representation of turbulent dispersing plumes. *J. Appl. Meteor.,* **33,** 721–732.

Tessier, Y., S. Lovejoy, and D. Schertzer, 1993: Universal multifractals: Theory and observations for rain and clouds. *J. Appl. Meteor.,* **32,** 223–250.

Voss, R. F., 1988: Fractals in nature: From characterization to simulation. *The Science of Fractal Images,* H.-O. Peitgen and D. Saupe, Eds., Springer-Verlag, 21–70.

Wilson, J., D. Schertzer, and S. Lovejoy, 1991: Continuous multiplicative cascade models of rain and clouds. *Non-Linear Variability in Geophysics,* D. Schertzer and S. Lovejoy, Eds., Kluwer, 185–207.